Light regulation of coccolithophore host–virus interactions

Kimberlee Thamatrakoln[1], David Talmy[2] (iD), Liti Haramaty[1], Christopher Maniscalco[1], Jason R. Latham[1], Ben Knowles[1], Frank Natale[1], Marco J. L. Coolen[3] (iD), Michael J. Follows[4] and Kay D. Bidle[1] (iD)

[1]Department of Marine and Coastal Sciences, Rutgers, The State University of New Jersey, 71 Dudley Road, New Brunswick, NJ 08901, USA; [2]Department of Microbiology, The University of Tennessee, Ken and Blaire Mossman Bldg, 1311 Cumberland Ave #307, Knoxville, TN 37996, USA; [3]WA Organic and Isotope Geochemistry Centre, School of Earth and Planetary Sciences, Curtin University, Bentley, WA 6102, Australia; [4]Department of Earth, Atmosphere and Planetary Sciences, MIT, Cambridge, MA 02139, USA

Summary

- Viruses that infect photoautotrophs have a fundamental relationship with light, given the need for host resources.
- We investigated the role of light on *Coccolithovirus* (EhV) infection of the globally distributed coccolithophore, *Emiliania huxleyi*. Light was required for EhV adsorption, and viral production was highest when host cultures were maintained in continuous light or at irradiance levels of 150–300 µmol m^{-2} s^{-1}. During the early stages of infection, photosynthetic electron transport remained high, while RuBisCO expression decreased concomitant with an induction of the pentose phosphate pathway, the primary source of *de novo* nucleotides. A mathematical model developed and fitted to the laboratory data supported the hypothesis that EhV replication was controlled by a trade-off between host nucleotide recycling and *de novo* synthesis, and that photoperiod and photon flux could toggle this switch.
- Laboratory results supported field observations that light was the most robust driver of EhV replication within *E. huxleyi* populations collected across a 2000 nautical mile transect in the North Atlantic.
- Collectively, these findings demonstrate that light can drive host–virus interactions through a mechanistic interplay between host metabolic processes, which serve to structure infection and phytoplankton mortality in the upper ocean.

Introduction

Virus infection is a primary mechanism of high lysis rates of phytoplankton populations (van Boekel *et al.*, 1992; Bratbak *et al.*, 1993; Brussaard *et al.*, 1995; Valiela, 1995; Agustí *et al.*, 1998). It is estimated that algal viruses turn over more than a quarter of the photosynthetically fixed carbon, fueling microbial foodwebs and short-circuiting carbon export to higher trophic levels and the deep sea (Fuhrman, 1999; Suttle, 2007) by releasing dissolved organic matter into the surrounding water. At the same time, viral-induced transparent exopolymer particle production (Joassin *et al.*, 2011; Vardi *et al.*, 2012) suggests infection may stimulate vertical sinking flux and enhance biological pump efficiency. Despite the impact on phytoplankton communities, viral-induced mortality is not routinely accounted for in models of ecosystem processes and carbon export, due to inadequate mechanistic and quantitative understanding of the environmental factors that regulate host–virus interactions.

Emiliania huxleyi and its associated *Coccolithovirus* (EhV) is a highly studied marine eukaryotic algal host–virus model system due to its ecological relevance and the availability of genetically diverse hosts and EhV strains in culture (Schroeder *et al.*, 2002; Bidle & Vardi, 2011). Massive spring blooms of *E. huxleyi* in the

North Atlantic (Townsend *et al.*, 1994; Tyrell & Merico, 2004) are routinely terminated by the giant, lytic, double-stranded DNA containing EhVs (Bratbak *et al.*, 1993; Schroeder *et al.*, 2002; Lehahn *et al.*, 2014; Laber *et al.*, 2018; Sheyn *et al.*, 2018), and studies have revealed that host–virus interactions are critically controlled through a lipid-based chemical arms race and subcellular regulation of autophagy and programmed cell death pathways (Bidle *et al.*, 2007; Vardi *et al.*, 2012; Rose *et al.*, 2014; Rosenwasser *et al.*, 2014; Schatz *et al.*, 2014; Sheyn *et al.*, 2016). These studies have collectively set the stage for detailed exploration into the environmental conditions that regulate key cellular pathways during infection.

As one of the most fundamental and readily measured resources in the ocean, light critically regulates *E. huxleyi* distribution, growth, and productivity, and in turn viral genome replication and virion production given the need for host resources (e.g. nucleotides, lipids, proteins, and energy). Decreased photosynthetic efficiency (Evans *et al.*, 2006; Bidle *et al.*, 2007) and increased nonphotochemical quenching (Llewellyn *et al.*, 2007) during EhV infection suggest an uncoupling of photosynthetic electron flow and impaired photophysiology (Evans *et al.*, 2006), findings that are supported by transcriptomic analysis of photosynthetic-related genes during infection (Rosenwasser *et al.*, 2014; Gilg *et al.*, 2016). However, the

mechanistic connection between light, EhV infection, and host metabolism has yet to be fully characterized.

Here, we investigated the role of light in regulating host metabolism and infection dynamics and developed a mathematical model that explicitly resolves and quantifies the relationship between light and viral production. The cellular and biochemical basis of this interaction, combined with quantitative statistical analyses, helped to explain the vertical distribution of EhV abundance in natural *E. huxleyi* populations collected across a 2000 nautical mile transect in the North Atlantic. Our findings highlight the importance of light-driven host subcellular processes in mediating viral infection of *E. huxleyi* and vertically structuring these interactions in nature.

Materials and Methods

Culture and virus maintenance

Emiliania huxleyi strain 374, obtained from the National Center for Marine Algae and Microbiota, was batch grown in f/2 medium −Si at 18°C. Cultures were maintained under different photoperiods (14 h : 10 h, light : dark (LD) or continuous light) at an irradiance level of 150 µmol m^{-2} s^{-1}, or on a 14 h : 10 h, LD cycle at different irradiance levels (25, 150, 300, 500, 1000 and 2000 µmol m^{-2} s^{-1}) for > 2 months before experiments and kept optically thin by frequent transfers (*c.* 2–4 d) to prevent self-shading. Cell abundance was determined using a Coulter Multisizer II (Beckman Coulter, Brea, CA, USA) or an InFlux Model 209S Mariner flow cytometer (BD Biosciences, Franklin Lakes, NJ, USA). *Coccolithovirus* strain EhV201 (hereafter referred to as EhV) was kindly provided by Dr Michael Allen (Plymouth Marine Laboratory). Viral lysates were obtained by infecting *E. huxleyi* at a virus to host ratio of *c.* 5–10, based on total virus abundance. Upon lysis, debris was removed by 0.45 µm pore-size polycarbonate filtration (Millipore, Burlington, MA, USA). Virus abundance was measured in 0.5% glutaraldehyde fixed samples using SYBR Gold (Molecular Probes, Eugene, OR, USA) and flow cytometry (Brussaard, 2004).

Viral infection

Exponentially growing *E. huxleyi* cultures were infected with EhV (virus-to-host ratio: 5), *c.* 1–2 h into the light phase, unless otherwise stated. In comparative experiments (e.g. LD vs continuous light or LD vs dark), infections were performed concurrently using the same stock of freshly propagated viral lysate. For dark experiments, EhV was added at the onset of the light period to allow adsorption and internalization. At the end of the light phase, a subset of the cultures was wrapped in foil and kept dark for the remainder of the experiment. Control cultures continued on the normal LD cycle. For 3-(3,4-dichlorophenyl)-1,1-dimethylurea (DCMU) experiments, 5 µM was added to control and infected cultures 24 h postinfection (hpi). Burst size was calculated by dividing the total number of viruses produced by the number of host cells lost (i.e. maximum host abundance minus final host abundance). Cell biomass was collected for enzyme activity measurements and immunoblots by filtration onto 47 mm diameter, 1.2 µm pore-size polycarbonate filters, snap frozen in liquid nitrogen, and stored at −80°C.

Photosynthetic measurements

Electron transfer rates and the maximum photosynthetic efficiency of photosystem II (PSII), expressed as F_v/F_m, were measured using a custom-built fast fluorescence induction and relaxation system (Gorbunov & Falkowski, 2005). The minimum (F_o) and maximum (F_m) fluorescence yields, F_v/F_m (($F_m - F_o$)/F_m for dark-adapted cells and $\Delta F'/F_m'$ under ambient light), and σ_{PSII} (the functional absorption cross-section of PSII) were calculated from the analysis of fluorescence induction at the microsecond time scale. The photosynthesis vs irradiance curves were reconstructed from measurements of electron transport rates ($P = E \times \sigma_{PSII} \times \Delta F'/F_m'$) as a function of ambient irradiance E (µmol m^{-2} s^{-1}).

Viral adsorption

Free, extracellular virus abundance was used as a proxy for adsorption, where the disappearance of viruses from the medium is as an indication of viral adsorption onto host cells. Nonspecific adsorption was assessed by adding viruses to cell-free media. A drop in free virus was detected within 5 min, but returned to initial concentrations after 15 min, suggestive of nonspecific adsorption, presumably to the wall of the flask, and subsequent release of viruses. Therefore, measurements earlier than 30 min were not used.

Pentose phosphate pathway activity

NADPH production by the two rate-limiting enzymes of the pentose phosphate pathway (PPP), glucose-6-phosphate dehydrogenase and 6-phosophogluconate dehydrogenase, was measured via a modified protocol (Tian *et al.*, 1994; Šindelář *et al.*, 1999). Filters were thawed and cells were scraped in TEM buffer (20 mM tris(hydroxymethyl)aminomethane hydrochloride (Tris-HCl), 1 mM EDTA, 2.5 mM magnesium chloride, pH 7) with a fresh razor blade, transferred to tubes, and sonicated three times on ice in 20 s intervals (Misonix; Microson, Farmingdale, NY, USA; power setting of 2–3). After centrifugation (4°C, 10 min, 20 817 *g*), the supernatant was assayed in 96-well microtitre plates in a total volume of 300 µl containing 100 µl of cell extract, 150 µM NADP$^+$ (Sigma-Aldrich), 3 mM glucose 6-phosphate (Santa Cruz Biotechnology, Dallas, TX, USA), 3 mM 6-phosphogluconate (Sigma-Aldrich), and TM buffer (100 mM Tris-HCl, 12.5 mM magnesium chloride, pH 8). Negative controls were cell extracts and TM buffer, without substrate or NADP$^+$. Enzyme activity was determined from the slope of the reaction, measured every 30 s at 340 nm (SpectraMax M3, Molecular Devices, San Jose, CA, USA) between 10 and 30 min, and an NADPH standard curve (Caymen Chemical, Ann Arbor, MI, USA). Protein concentrations were determined using a BCA Protein Assay Kit (Thermo Fisher Scientific, Waltham, MA, USA).

Quantitative immunoblot analysis

Protein extraction and quantitative immunoblots were performed as described (Brown *et al.*, 2008; Thamatrakoln *et al.*, 2013). Immunoblots were probed with primary antibodies (Agrisera, Vännäs, Sweden) against PsbD (a proxy for PSII) and RbcL (a proxy for RuBisCO) at a dilution of 1 : 40 000, followed by a horseradish-peroxidase-conjugated secondary antibody at 1 : 10 000 dilution. Chemiluminescence detection was performed using ECL Select (GE Healthcare, Chicago, IL, USA) and imaged using a Chemidoc XRS+ CCD imager (Bio-Rad, Hercules, CA, USA). Adjusted volume values were obtained, and standard curves of serially diluted recombinant proteins were used to estimate the amount of protein as described (Brown *et al.*, 2008; Thamatrakoln *et al.*, 2013).

Nonlinear model of host–virus nucleotide dynamics

A mathematical model was developed to characterize and disentangle the effect of host growth, host nucleotide recycling and *de novo* nucleotide synthesis on host–virus population dynamics. By extension to Wikner *et al.* (1993), the model resolves time variation in the concentration of nucleotides (nucleotides ml^{-1}) within uninfected hosts (S), infected hosts (I), internal viruses produced by host nucleotide recycling (P), internal viruses produced by *de novo* nucleotide synthesis (D), and free (extracellular) viruses (V). Direct measures of the individual nucleotide pools were not made given methodological limitations. Rather, the model was constrained with total cellular nucleotides ($S + I + P$) and free viral nucleotides (V), which were converted from host and virus abundance respectively and known genome size (Supporting Information Table S1). We hypothesized that host growth, nucleotide recycling and *de novo* synthesis each have a distinct and quantifiable influence on the dynamics of total cellular and free viral nucleotides and that these distinct signatures would lead to constraint on the light dependence of nucleotide synthesis rates. Parameter definitions and units are in Table S1.

$$\frac{\mathrm{d}S}{\mathrm{d}t} = \underbrace{\mu_\mathrm{h} S}_{\text{host growth}} - \underbrace{(1 - v_\mathrm{x})\phi SV}_{\text{adsorption}} \qquad \text{Eqn 1}$$

$$\frac{\mathrm{d}I}{\mathrm{d}t} = \underbrace{\mu_\mathrm{h} I}_{\text{host growth}} + \underbrace{(1 - v_\mathrm{x})\phi SV}_{\text{adsorption}} - \underbrace{v_\mathrm{p}\mu_\mathrm{v} I}_{\text{nucleotide recycling}} - \underbrace{v_\mathrm{p}\delta I}_{\text{lysis}}$$

$$\text{Eqn 2}$$

$$\frac{\mathrm{d}P}{\mathrm{d}t} = \underbrace{v_\mathrm{p}\mu_\mathrm{v} I}_{\text{nucleotide recycling}} - \underbrace{v_\mathrm{p}\delta P}_{\text{lysis}} \qquad \text{Eqn 3}$$

$$\frac{\mathrm{d}D}{\mathrm{d}t} = \underbrace{v_\mathrm{p}\mu'_\mathrm{v} I}_{\text{\textit{de novo} synthesis}} + \underbrace{v_\mathrm{x}\phi SV}_{\text{adsorption}} - \underbrace{v_\mathrm{p}\delta D}_{\text{lysis}} \qquad \text{Eqn 4}$$

$$\frac{\mathrm{d}V}{\mathrm{d}t} = - \underbrace{v_\mathrm{x}\phi SV}_{\text{adsorption}} + \underbrace{v_\mathrm{p}\delta(P + D)}_{\text{lysis}} \qquad \text{Eqn 5}$$

In Eqn 1, hosts synthesize nucleotides at rate μ_h. The linear interaction term ϕSV, controls the total flux of nucleotides from susceptible hosts and free, extracellular viruses to newly synthesized, intracellular viruses. The parameter v_x represents the portion of this flux that originates from the virus, and $1 - v_\mathrm{x}$ represents the portion that originates from the host, with

$$v_x = \frac{V_\mathrm{ind}}{V_\mathrm{ind} + S_\mathrm{ind}} \qquad \text{Eqn 6}$$

where V_ind and S_ind are the nucleotide contents of an individual virus and host respectively (Table S1).

In Eqn 2, infected hosts synthesize nucleotides at rate μ_h, and nucleotides are either converted to viral progeny at rate $v_\mathrm{p}\mu_\mathrm{v}$ or lysed at rate $v_\mathrm{p}\delta$. The parameter v_p is included to mimic a delay in internal viral production and host lysis due to internal assembly of viral progeny. This delay parameterizes the latent period (i.e. the time during which the virus is replicating prior to host lysis). Unlike previous models that mimic the latent period with a time lag (e.g. Wang, 2006), v_p forces a delay due explicitly to the internal depletion of host resources by the virus. Specifically, v_p forces the rate of lysis to increase as host resources are converted to intracellular viruses:

$$v_\mathrm{p} = \frac{P + D}{I + P + D} \qquad \text{Eqn 7}$$

In Eqn 7, as host nucleotides I are converted to internal viral nucleotides $P + D$, v_p increases from very low values and then saturates close to one, which in turn causes the rate of lysis $v_\mathrm{p}\delta$ in Eqn 2 to increase, and then saturate at a fixed rate.

Nucleotides required for viral genome replication can be obtained in two ways, either through recycling of existing host nucleotides or *de novo* nucleotide synthesis. Recycling, by definition, leads to a depletion of host nucleotides, whereas *de novo* synthesis does not. Eqn 3 accounts for the accumulation of internal viruses by nucleotide recycling at rate $v_\mathrm{p}\mu_\mathrm{v}$, and the loss of internal viruses due to lysis at rate $v_\mathrm{p}\delta$. Eqn 4 accounts for the production of internal viruses by *de novo* synthesis at rate $v_\mathrm{p}\mu'_\mathrm{v}$, as well as accumulation of internal viruses due to adsorption, and losses due to host lysis at rate $v_\mathrm{p}\delta$. Having the rate of nucleotide recycling and *de novo* nucleotide synthesis dependent on v_p accounts for the time it takes for a virus to co-opt the host biosynthetic machinery. Note that the sum of Eqns 3 and 4 represents a single mass balance for the total number of internal nucleotides, $P + D$. We separate P and D because it is only appropriate to count nucleotides generated via recycling P, with host nucleotides inferred with measured cell abundance and known nucleotide content (i.e. genome size; Table S1). Nucleotides generated via *de novo* synthesis are assumed to be 'invisible' until host lysis.

Eqn 5 assumes the free virus nucleotide concentration V is a balance between production of free viruses by host lysis at rate $v_p\delta$, and uptake of viruses due to adsorption to host cells at rate $v_x\phi S$. For all experiments, model solutions were obtained by numerically integrating Eqns 1–5 using initial conditions that matched the experimental observations.

Parameter constraint with the Metropolis algorithm

Our goal was to quantify the effect of host growth, nucleotide recycling and *de novo* nucleotide synthesis on total cellular ($S + I + P$) and free viral (V) nucleotide dynamics. We used the Metropolis algorithm (Metropolis *et al.*, 1953) to test formally whether rates of nucleotide synthesis could be uniquely constrained with knowledge of total cellular and free-virus dynamics. We leveraged this constraint to explore the light dependence of viral replication. The Metropolis algorithm is a Monte Carlo type simulation that quantifies parameter uncertainty using a random walk to explore parameter combinations that explain observed dynamics. When the observations are unable to constrain model parameters, the random walk does not converge, and the algorithm predicts ever wider parameter distributions. When the observations are sufficient to constrain model parameters, the algorithm converges on unique parameter distributions.

The five model parameters controlling infection dynamics are virus adsorption ϕ, host growth rate μ_h, host nucleotide recycling rate μ_v, *de novo* nucleotide synthesis rate μ'_v, and lysis rate δ. The adsorption parameter was fitted using data from adsorption experiments. The remaining parameters $\theta = \{\mu_h, \mu_v, \mu'_v, \delta\}$ were fitted using population-level observations, labeled here $D(t_i)$, of host–virus dynamics. The Metropolis algorithm starts with an initial parameter set $\theta_{current}$ manually determined so that the model solutions are reasonably close to the observations. A new parameter set, $\theta_{proposed}$, is then drawn from appropriate distributions. We used lognormal distributions with means matching the old distribution, and standard deviations chosen manually to ensure average acceptance ratios within the range 23–44% to promote efficient convergence (Gelman *et al.*, 1996). The new parameters were chosen from lognormal distributions to prevent negative values. Solutions $y(t_i|\theta_{proposed})$ to the model with the new parameter set are then calculated. For both the old and the new models, the sum-of-squared difference between the model and the observations is divided by the measurement uncertainty of the observations, assumed here to be the average variance of each triplicate σ^2.

$$\chi^2_{current} = \sum_i \frac{D(t_i) - y(t_i|\theta_{current})}{2\sigma^2} \qquad \text{Eqn 8}$$

$$\chi^2_{proposed} = \sum_i \frac{D(t_i) - y(t_i|\theta_{proposed})}{2\sigma^2} \qquad \text{Eqn 9}$$

A likelihood function is defined in the following way:

$$P(D|\theta) = \exp(-\chi^2) \qquad \text{Eqn 10}$$

A likelihood ratio is then calculated by taking the ratio of the new to the old likelihood function:

$$\frac{P(D|\theta_{proposed})}{P(D|\theta_{current})} = \exp(-\chi^2_{proposed} + \chi^2_{current}) \qquad \text{Eqn 11}$$

If the likelihood ratio is larger than a random number r between 0 and 1, the new parameter set becomes $\theta_{current}$, and the process is repeated. If the likelihood ratio is less than r, the proposed set of parameters is disregarded and the process repeated with the old parameter set. Whenever a new parameter set is adopted, those parameters are recorded. Over time, enough parameters are stored to estimate parameter distributions that minimize error between the model and the observations. The distributions represent the full range of parameters that give suitable fits with respect to uncertainty in the observations.

By repeating the fitting exercise for both the light and the dark treatments, estimates of parameter distributions for μ_h, μ_v, μ'_v, and δ were generated. All simulations were repeated numerous times from different initial parameter guesses to ensure consistent convergence. Parameters were assumed to be constrained by the data if the variance in the posterior distribution did not increase with respect to the number of iterations of the optimization algorithm. In some cases, this led to poor constraint; for example, in the continuous light treatments. By looking for differences in the fitted parameter distributions between different light treatments, we were able to discern whether key processes, namely *de novo* synthesis or recycling of host nucleotides, were dependent on light intensity.

Field sampling and statistical analysis

Emiliania huxleyi populations (and associated EhVs) were collected during the North Atlantic Virus Infection of Coccolithophores Expedition (http://www.bco-dmo.org/project/2136) using Niskin bottles on a 24-position rosette equipped with an SBE conductivity–temperature–depth profiler (Sea-Bird Scientific, Bellevue, WA, USA). Cell biomass (and associated viruses) was collected from *c.* 3–5 l of 200 μm mesh-filtered seawater onto large (142 mm diameter), 0.8 μm pore-size polycarbonate filters (Millipore) to minimize clogging. Filters were immediately submerged in 10 ml extraction buffer (100 mM Tris-HCl pH 8, 250 mM EDTA pH 8, 100 mM sodium chloride, and 1% sodium dodecyl sulfate) and homogenized at maximum speed on a Vortex Genie (Mo Bio, Carlsbad, CA, USA) for 10 min in the presence of 2 ml molecular-grade zirconium beads (equal amount of 100 μm and 400 μm diameter beads; OPS Diagnostics, Lebanon, NJ, USA). Filters were subjected to three freeze–thaw cycles via submerging in liquid nitrogen and thawing at 50°C, homogenized for 5 min after each cycle and stored at −80°C. Upon processing, filters were thawed and 5 ml was incubated for 1 h at 50°C with 100 μg Proteinase K, followed by phenol : chloroform : isoamyl alcohol, 25 : 24 : 1 v/v/v extraction. Nucleic acids were precipitated with two volumes of 100% ethanol and 0.2 M sodium chloride. Following centrifugation (20 min, 10 000 *g*), the DNA

pellet was washed with 20 ml of 70% ethanol, centrifuged again (10 min, 10 000 g) and then resuspended in 1× TE buffer (pH 8). Trace impurities that could inhibit enzymatic amplification reactions were removed using the PowerClean® DNA Clean-Up Kit (Mo Bio). Quantitative PCR using SYBR®Green was used to quantify *E. huxleyi* (via cytochrome oxidase I) and EhV (via major capsid protein) (Coolen, 2011). Tenfold serially diluted genomic DNA (extracted from flow cytometry quantified *E. huxleyi* (RCC1216) and EhV (EhV86) was used to calibrate the cytochrome c oxidase I- and major capsid protein-specific quantitative PCR. Data were analyzed by linear regression in R using the lm() function and model fit verified with the plot(-model) function. All data were log$_{10}$-transformed for consistency.

Results

EhV infection, the PPP, and photosynthesis

Genes associated with *de novo* nucleotide synthesis, namely those involved in the PPP, were found to be upregulated during infection of *E. huxleyi* (Rosenwasser *et al.*, 2014). To determine whether these observed increases in transcript abundance translated into higher rates of nucleotide synthesis, we measured the enzymatic activity of key enzymes of the PPP during the early stages (< 24 hpi) of EhV infection. EhV infection arrested host growth within 24 hpi, concomitant with an increase in the production of extracellular viruses (Fig. S1). PPP activity in uninfected controls remained steady at *c.* 9 nM NADPH min^{-1} µg protein^{-1} (Table 1). In contrast, PPP activity increased in infected cultures by *c.* 1.6-fold between 4 and 14 hpi, reaching maximum levels that were > 2.5-fold higher than uninfected controls by 24 hpi. Given that the PPP shares enzymes with the Calvin cycle, upregulation of the former should result in the downregulation of the latter. Measured protein expression levels of RuBisCO (Fig. 1a), the rate-limiting enzyme of the Calvin cycle, showed that the induced PPP activity was coincident with a 50% decrease in the biochemical potential of the Calvin cycle. In contrast, PsbD (a proxy for PSII) protein expression was similar between control and infected cells (Fig. 1a), suggesting photosynthetic electron transport was not inhibited in infected *E. huxleyi*.

No significant difference was observed in the electron transport rate between control and infected cells 5 hpi (data not shown) or 24 hpi (Fig. 1b). We further tested the role of PSII in viral production by inhibiting PSII activity with DCMU (Fig. 1c). There was a *c.* 15% drop in cell abundance in infected cultures that was not observed in infected cultures without

DCMU (Fig. 1c, inset). Associated viral abundance was reduced by *c.* 50% in infected cultures treated with DCMU (Fig. 1d), which was not due to lower host growth, as the decrease in host abundance in the presence of DCMU was less (*c.* 30%) than the accompanying decrease in viral production. The infection was carried out for an additional 48 h to assess whether viral replication in DCMU-treated cultures was delayed, but cultures failed to produce the equivalent number of viruses as untreated, infected cultures, even at 96 hpi.

Light critically regulates infection

Light heavily impacted virus adsorption to *E. huxleyi* cells. There was little adsorption when EhVs were added to *E. huxleyi* at the onset of the dark period (see the Materials and Methods section). Only upon transition to the light 10 h later was there notable adsorption, observed as a 78% drop in free EhV abundance within 2 h (Fig. 2a). By contrast, when EhV was added at the onset of the light period, a near immediate drop of 44% in free EhV abundance was observed (Fig. S2a), consistent with previous studies (Mackinder *et al.*, 2009).

EhV production, defined as the number of EhVs measured upon lysis, was also light dependent. Comparative infection dynamics in the dark were performed after EhV was allowed time to adsorb to host cells in the light. Although uninfected *E. huxleyi* cultures did not grow in the dark (Fig. 2b), cell lysis and declines in host abundance were observed for both infected cultures regardless of light or dark treatment (Fig. 2b). However, the 71% lower virus production in the infected, dark treatment (Fig. S2b) resulted in a 3.5-fold lower burst size (i.e. the number of viruses produced per *E. huxleyi* cell) compared with infected cultures grown on an LD cycle (Fig. 2c).

Under continuous light, *E. huxleyi* growth and F_v/F_m were similar to cultures grown on a LD cycle (Figs 2d, S2c), indicating cells were not physiologically stressed, consistent with previous observations (Nielsen, 1997). However, infected cultures under continuous light produced *c.* 50% more viruses (Fig. S2d), resulting in a 1.5-fold higher burst size (Fig. 2e). Infected cultures in continuous light also had nearly twofold higher PPP activity than LD infected cultures (average over the entire experiment was 4.7 ± 1.4 nM $^{-1}$ and 2.5 ± 0.6 nM NADPH min^{-1} µg protein^{-1} respectively), with significant increases observed as early as 6 hpi under continuous light compared with 20 hpi under LD conditions (Fig. 2f,g).

We also tested how photon flux impacted host–virus interactions. The maximum steady-state growth rate μ_{max} at irradiance

Table 1 NADPH production rate with time, hours postinfection (hpi), in control and infected *Emiliania huxleyi* cultures.

	NADPH production rate (nM min^{-1} µg protein^{-1})				
	4 hpi	14 hpi	19 hpi	24 hpi	28 hpi
Control	10.9 ± 0.9	9.1 ± 0.3	8.4 ± 0.9	9.2 ± 0.4	7.2 ± 1.4
Infected	10.6 ± 0.2	14.0 ± 1.9*	18.4 ± 2.3*	26.1 ± 1.3**	23.6 ± 1.5**

Mean ± SD for biological triplicates is shown; *t*-test: *, $P < 0.01$; **, $P < 0.001$.
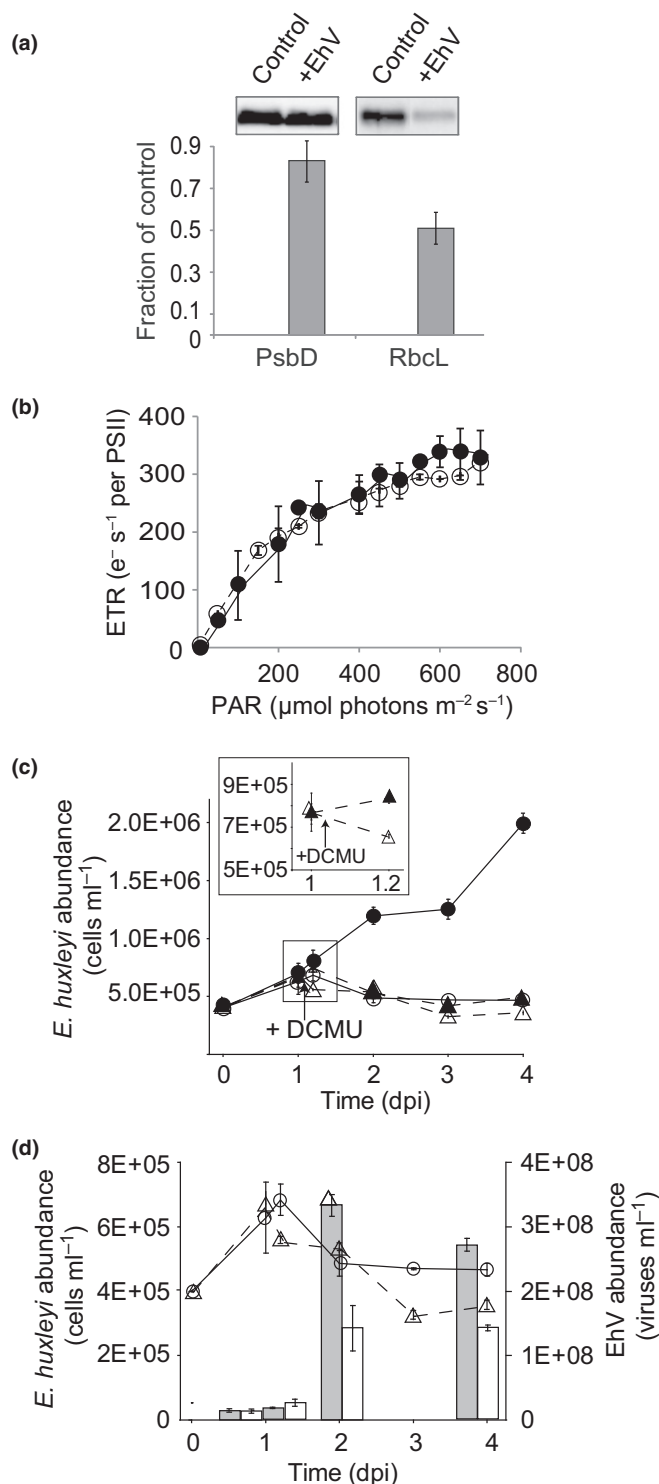
(a)

(b)

(c)

(d)

Fig. 1 Characterization of photosynthesis during infection. (a) Quantitative immunoblot of PsbD and RbcL in a control and infected culture 24 h postinfection (hpi). Bar graph shows the fraction of expression in infected cultures compared with control in three biological replicates with the percentage $\pm$ SE denoted by the error bars. Data are representative of two independent experiments. (b) Electron transfer rate (ETR) 24 hpi in two independent cultures of control (closed circles, solid line) and infected (open circles, dashed line). (c) Host abundance during infection in the presence of 3-(3,4-dichlorophenyl)-1,1-dimethylurea (DCMU). *Coccolithovirus* (EhV) was added to cultures of *Emiliania huxleyi* (open circles and triangles) at $t = 0$ and allowed to adsorb and enter into host cells. Uninfected cultures are denoted by closed circles and triangles. After 24 hpi ($t = 1$ d), 5 μM DCMU was added to both uninfected (closed triangles) and infected cultures (open triangles). Inset: host abundance before ($t = 1$ d) and after ($t = 1.2$ d) DCMU addition. (d) EhV abundance in cultures with (open bars) and without (closed bars) DCMU. Host abundance of infected (open circles) and infected + DCMU (open triangles) are shown for reference. Data are mean $\pm$ SD for triplicate cultures. PAR, photosynthetically active radiation; dpi, days postinfection.

of 2000 μmol m^{-2} s^{-1} suggests the decreased growth may have been due to impaired photophysiology. When infected at an irradiance of 25, 150 or 300 μmol m^{-2} s^{-1}, host lysis occurred *c.* 4 d postinfection (dpi; Fig. 3b). By contrast, lysis occurred within 2–3 dpi at an irradiance > 500 μmol m^{-2} s^{-1} (Fig. 3b). EhV production was maximal at intermediate irradiance (150 and 300 μmol m^{-2} s^{-1}, Fig. 3c) and was approx. five-fold lower at irradiances of 25 and 500 μmol m^{-2} s^{-1}, and 16-fold lower at irradiances of 1000 and 2000 μmol m^{-2} s^{-1} (Fig. 3c). When expressed as a burst size, the intermediate irradiance levels produced the highest number of viruses per host (Fig. 3d). This relationship was robust, being observed across a large number ($n = 5$–25) of discrete samples (Fig. S3).

Photoperiod and irradiance serve as a switch between *de novo* and recycled nucleotide synthesis

Given the increased PPP activity concomitant with decreased RuBisCO expression, we hypothesized enhanced viral production in the light was due to a concerted strategy to increase nucleotide synthesis and viral genome replication, while maintaining host integrity. To test this, we developed a mathematical model to quantify the dependence of free virus population dynamics on the rate of *de novo* nucleotide synthesis (Eqns 1–5; Fig. S4), accounting for the potentially interacting and compensating effects of host growth and recycling of host material. Our premise was that host growth μ_h, nucleotide recycling μ_v and *de novo* nucleotide synthesis μ'_v each have distinct and constrainable effects on population dynamics. We leveraged the dependence of host–virus population dynamics on these internal processes to infer their light dependence.

In Fig. 4 we show the contrasting effect within the model of nucleotide recycling μ_v and *de novo* nucleotide synthesis μ'_v on population dynamics. Increasing the rate of nucleotide recycling leads to an earlier decline of the host population (Fig. 4a) and

levels of 150, 300, and 500 μmol m^{-2} s^{-1} was similar (*t*-test *P*-value > 0.05; in the range 0.89–0.96 $\pm$ 0.10–0.14 d^{-1}), whereas μ_{max} was 0.45 $\pm$ 0.09 d^{-1} and 0.74 $\pm$ 0.10 d^{-1} at irradiance levels of 25 μmol m^{-2} s^{-1} and 2000 μmol m^{-2} s^{-1} respectively (Fig. 3a). At all irradiance levels except 2000 μmol m^{-2} s^{-1}, F_v/F_m was similar, suggesting growth at an irradiance of 25 μmol m^{-2} s^{-1} was limited by light rather than impaired photosynthetic efficiency (Fig. 3a). The lower F_v/F_m at an irradiance
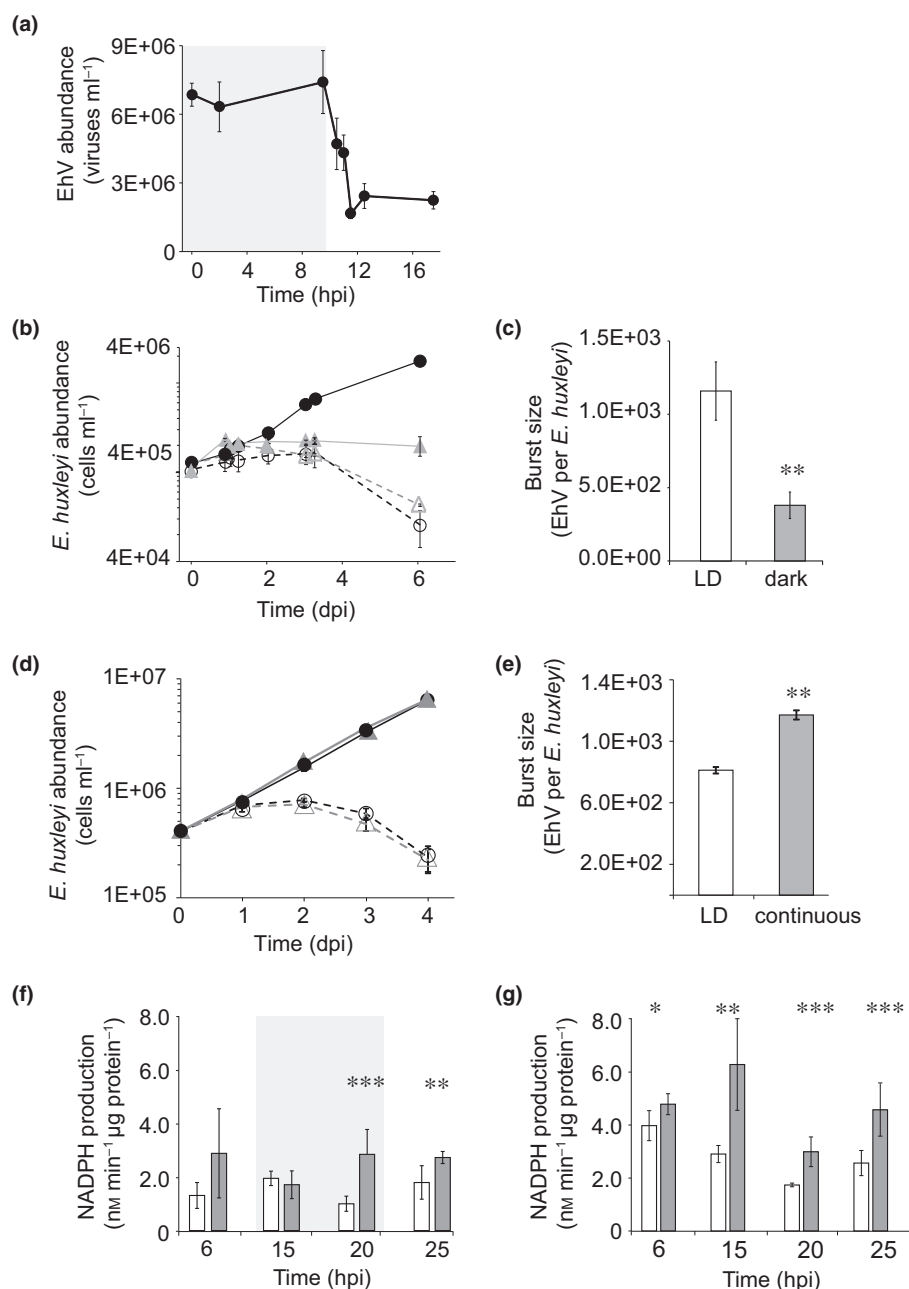
Fig. 2 The role of light in mediating adsorption and infection dynamics. (a) *Coccolithovirus* (EhV) was added at the onset of the dark phase ($t = 0$ h), delineated by the grey shading. Free, extracellular EhV abundance was followed throughout the dark and 7 h after the transition to the light. Data are the mean ± SD of triplicate cultures and are representative of two independent experiments. (b) *Emiliania huxleyi* abundance in control and infected cultures on a 14 h : 10 h, light : dark (LD) cycle (black lines) or maintained in complete darkness (gray lines). Solid and dashed lines represent uninfected and infected cultures, respectively. Note: y-axis is on a log scale. (c) Burst size (the number of viruses produced per host cell) for LD (white bar) and dark (gray bar) infected culture calculated 6 d postinfection (dpi). Data shown are mean ± SD for triplicate cultures and are representative of two independent experiments. (d–g) Host and viral abundance and pentose phosphate pathway (PPP) activity in *E. huxleyi* growing on a 14 h : 10 h LD cycle or under continuous light. (d) Host abundance of cultures grown on a 14 h : 10 h LD cycle (black lines) or continuous light (gray lines). Solid and dashed lines represent uninfected and infected cultures respectively. Note: y-axis is on a log scale. (e) Burst size in LD and continuous light-infected cultures calculated at 4 dpi. Data are mean ± SD of duplicate cultures within a single experiment and are representative of two independent experiments. (f) Time course of NADPH production via PPP enzyme activity in control (white bars) and infected (gray bars) cultures on a 14 h : 10 h LD cycle with the gray shading denoting the dark period, or (g) under continuous light. Means ± SDs are shown for triplicate cultures. Significance between control and infected cultures was determined using a *t*-test: *, $P < 0.05$; ** $P < 0.01$; *** $P < 0.001$.

lower viral production due to the premature lysis of the host (Fig. 4b). Increased *de novo* synthesis also leads to early host decline (Fig. 4c) but results in enhanced viral production

(Fig. 4d). The early decline of the host with increased *de novo* nucleotide synthesis is a consequence of our assumption that the rate of lysis is influenced positively by the accumulation of
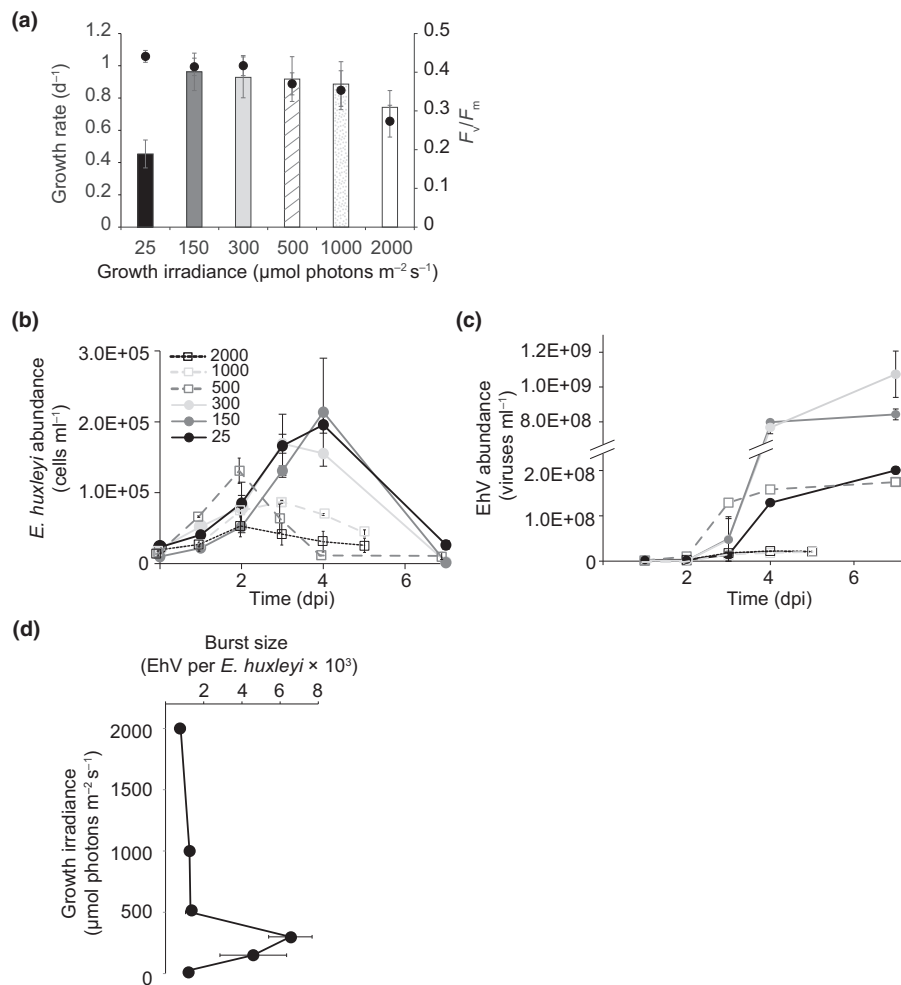
Fig. 3 The impact of irradiance level on host growth and viral infection. (a) Growth rate (bars) and F_v/F_m (circles) of cultures of *Emiliania huxleyi* acclimated and grown at light irradiance level of 25, 150, 300, 500, 1000 or 2000 μmol m^{-2} s^{-1}. (b) Time course of *E. huxleyi* abundance, postinfection with *Coccolithovirus* (EhV) at $t = 0$ d at the different light irradiances. Uninfected controls are not shown for simplicity. (c) Time course of EhV abundance at different light irradiance levels. (d) Burst size was calculated at the final timepoint for each light irradiance and plotted as a function of growth irradiance similar to a depth profile where higher irradiance would represent surface depths and lower irradiance would be closer to the base of the euphotic zone. Data are mean ± SE of duplicate cultures, except for data from light irradiance levels 500 and 1000 μmol m^{-2} s^{-1}, which are from triplicate cultures. Data shown are from a single experiment but are representative of two to four independent experiments. Note that gradient shading of bars, lines, and symbols reflects the relative light levels (from dark to light).

internal viral nucleotides (Eqns 3–5, 7). However, the concomitant increase in the rate of *de novo* nucleotide synthesis allows increased viral production. The contrasting dynamics in Fig. 4(a, b) and Fig. 4(c,d) respectively provide a distinct signature that allows the model to make predictions about nucleotide recycling μ_v and *de novo* synthesis μ'_v, based on host and virus population dynamics.

To assess the light dependence of these rates, we first assessed whether the model with these assumptions was consistent with the observed host–virus population dynamics. We then asked, using a formal fitting procedure with explicit quantification of parameter uncertainty (Metropolis *et al.*, 1953), whether there were clear differences in rates of recycling and *de novo* nucleotide synthesis between light treatments.

The model successfully captured host–virus nucleotide dynamics in cultures infected in the dark, on an LD cycle, and under continuous light (Fig. S5). For the dark and LD treatments, the

Metropolis algorithm converged on unique parameter distributions (Fig. 5), demonstrating that the empirical measurements were sufficient to constrain model parameters in these conditions. The continuous light treatment had too few measurements to constrain parameter values (Fig. S5e,f).

The model output suggests that host nucleotide recycling and *de novo* nucleotide synthesis were both strongly dependent on light, and the contribution of nucleotides to viral genome replication by each pathway could be toggled by external light conditions. In dark treatments, the model predicted rapid nucleotide recycling, accompanied by relatively slow *de novo* synthesis (Fig. 5a,b). This prediction is due to rapid demise of host populations in the dark and low viral production (Figs 2b, 4a,b). Conversely, LD treatments showed slower recycling and more rapid *de novo* synthesis (Fig 5a,b), arising from delayed host lysis and a large burst of free-virions toward the end of the infection (Figs 2, 4c,d).
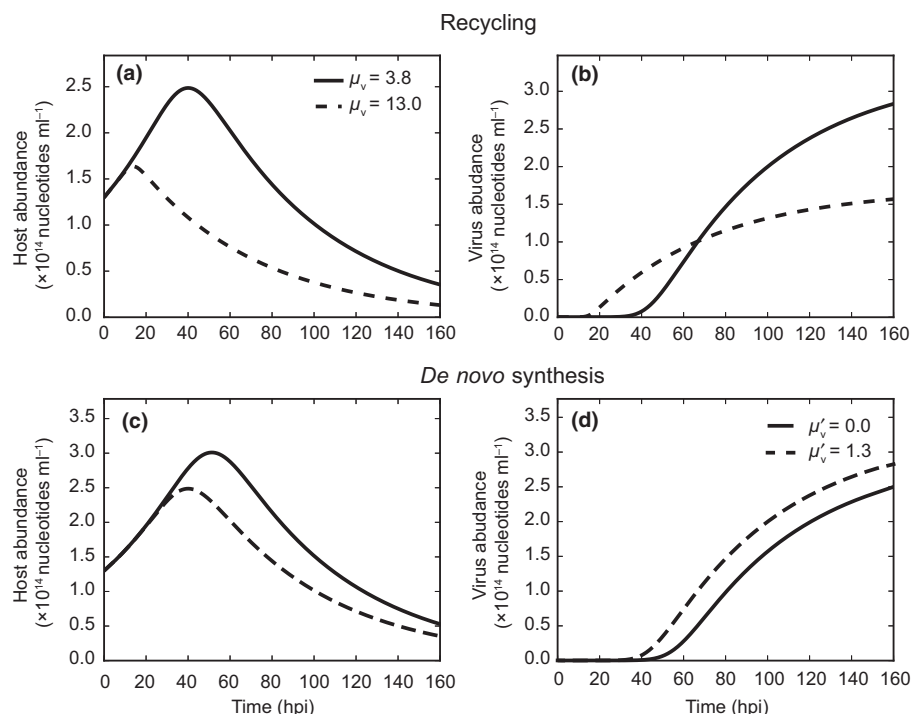
Recycling

Fig. 4 Sensitivity analysis of infection dynamics to the rate of host nucleotide recycling μ_v and *de novo* synthesis μ'_v during the time-course of infection. When a higher rate of nucleotide recycling is assumed, (a) host abundance declines more rapidly and (b) free, extracellular virus abundance decreases. When a high rate of *de novo* synthesis is assumed, (c) host abundance declines more rapidly due to faster internal progression of infection and (d) viral abundance increases. The distinct signature of these parameters on host–virus population dynamics allows their light dependence to be quantified.
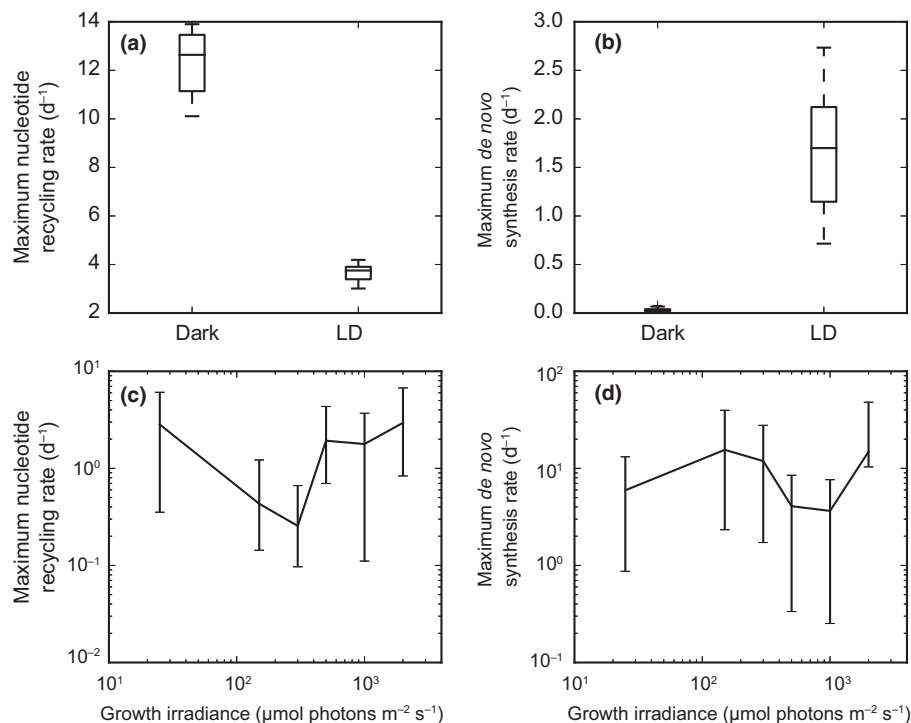

Fig. 5 Rates of viral-mediated recycling of host nucleotides and *de novo* nucleotide synthesis are sensitive to irradiance level. Parameter estimates for the rates of host nucleotide recycling or *de novo* synthesis, obtained using the Metropolis algorithm to fit Eqns 1–5 to *Emiliania huxleyi*–*Coccolithovirus* nucleotide dynamics shown in Supporting Information Fig. S4. (a, b) Maximal recycling μ_v and *de novo* synthesis μ'_v in dark and light : dark (LD) treatments. Box edges are lower and upper quartiles, and whiskers are 5th and 95th quartiles of the posterior parameter distributions. (c, d) Estimates of μ_v and μ'_v for irradiance level experiments. Error bars are lower and upper quartiles either side of the medians.
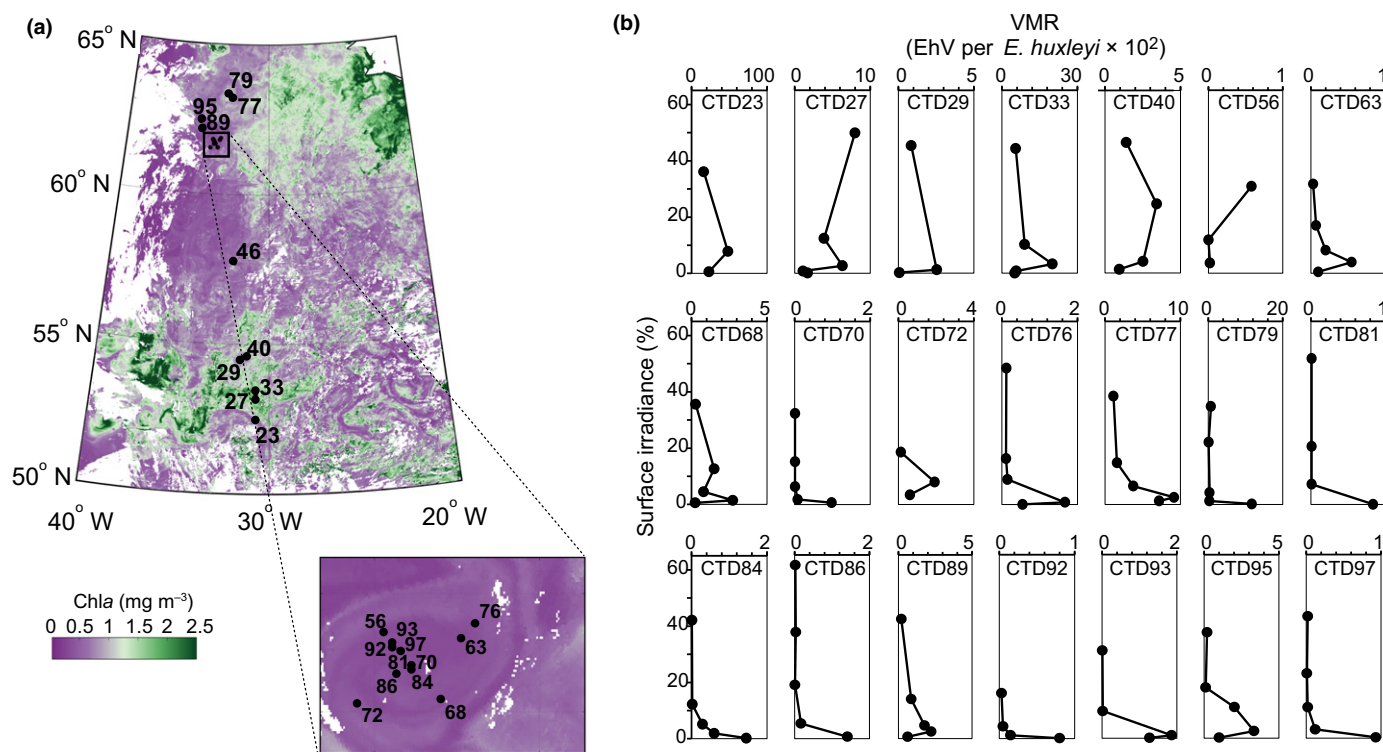
Fig. 6 Light structures the *Coccolithovirus* (EhV) : *Emiliania huxleyi* ratios in natural populations collected in the North Atlantic during the summer of 2012. (a) Map of conductivity–temperature–depth (CTD) stations overlaid on 18 d surface averaged Chl concentrations obtained by satellite. (b) Depth profile of the intracellular virus-to-microbe ratio (VMR), determined by quantitative PCR, at 21 stations across the North Atlantic. Percentage of surface irradiance is shown on the *y*-axis with VMR on the *x*-axis.

Contrasting parameter predictions during LD vs dark treatments were insensitive to a wide range of virus adsorption rates ϕ, suggesting predictions of *de novo* synthesis and recycling rates are robust to any uncertainty in our predictions of ϕ (Fig. S6).

Repeating the fitting procedure for experiments at different light intensities revealed that the rate of nucleotide recycling and *de novo* synthesis were also strongly dependent on irradiance level. Nucleotide recycling was lowest at intermediate irradiance (150–500 μmol m^{-2} s^{-1}) and highest at low and high irradiances (25, 1000–2000 μmol m^{-2} s^{-1}; Fig. 5c). *De novo* synthesis was opposite, being the highest at intermediate irradiance and lowest at low and high irradiance (Fig. 5d). In some cases, predictions of recycling and *de novo* synthesis rates were poorly constrained by the experimental data (Fig. 5c,d), but the clear difference across light intensities in spite of this large error supports the hypothesis that key infection parameters are light dependent. Taken together, these model predictions demonstrate that slow recycling and rapid *de novo* synthesis combine to impact EhV production and that light can lead to a systematic shift between nucleotide recycling and *de novo* synthesis.

Light structures infection of natural populations

The termination of dense coastal and open ocean North Atlantic blooms of *E. huxleyi*, which can span 10^5 km^2 (Holligan *et al.*, 1993; Tyrell & Merico, 2004) and last over a period of days to

weeks, is commonly attributed to EhV infection (Bratbak *et al.*, 1993; Vardi *et al.*, 2012; Lehahn *et al.*, 2014). We used the 2012 North Atlantic Virus Infection of Coccolithophores Expedition as a platform to extend our laboratory-based mechanistic findings and test the hypothesis that irradiance structures the infection of natural populations of *E. huxleyi*. We previously demonstrated these populations were at various stages of infection (Laber *et al.*, 2018) using a suite of structurally distinct glycosphingo- and betaine-like lipids that represent functional biomarkers of the *E. huxleyi*–EhV infection process (Vardi *et al.*, 2009, 2012; Fulton *et al.*, 2014; Hunter *et al.*, 2015). Using targeted, quantitative PCR we quantified the intracellular abundance of *E. huxleyi*-associated EhVs (expressed as a virus-to-microbe ratio, VMR) at three to five depths (97 discrete samples) in the euphotic zone at 21 stations across the *c.* 2000 nautical mile cruise track (Figs 6, S7). At 18 of the 21 stations, there was a subsurface VMR maximum that corresponded to *c.* 1–10% of the surface irradiance I_0. The relationship between VMR and percentage surface I_0 (Fig. 6b) at these stations was similar to that between burst size and irradiance level seen in laboratory cultures (Fig. 3d), in that there was an optimal percentage surface I_0 that supported the highest VMR; above and below that optimum, VMR decreased. Taking the entire dataset together, there was a significant positive relationship between VMR and depth ($P = 6.19 \times 10^{-4}$, slope 0.02, $R^2 = 0.12$; linear regression with log-transformed VMR and depth), despite the inherent variability in pooling across stations. These observations corroborate active, subsurface infection of these populations (Laber *et al.*,

Table 2 Statistical analysis of North Atlantic environmental samples collected during the North Atlantic Viral Infection of Coccolithophores Expedition.

Parameter	Units (log$_{10}$)	P-value	Slope	R^2	n	Outliers?
Physical						
Depth	m	**6.19 × 10^{-4}**	0.02	0.12	97	No
Light	Surface irradiance (%)	**5.42 × 10^{-5}**	−0.44	0.15	97	No
Salinity	PSU	> 0.1	−29.01	0.03	97	Yes
Mixed-layer depth	m	0.24	0.82	0.015	97	No
Temperature	°C	0.91	0.75	0.01	97	No
Chemical						
Nitrate and nitrite	μM	0.29	−0.42	0.012	94	Yes
Ammonium	μM	0.57	0.19	0.004	97	No
Phosphate	μM	0.30	0.22	0.014	81	Yes
Dissolved O$_2$	ml l^{-1}	0.02	−5.73	0.06	97	Yes

All stations from the cruise were pooled within each analysis to probe the prediction from laboratory studies that the intracellular virus-to-microbe ratio (VMR) would vary with depth. Subsequent analyses examined which component of depth (physical or chemical) drives this relationship. All data were analyzed by linear regression against the VMR, with both predictors and VMR log-transformed; parameter, units, significance (P-value), slope, goodness of fit (R^2), and sample size (n) of regression lines, and the presence of outlying values are shown. Bold P-values are those with significance < 0.001.

2018; Sheyn *et al.*, 2018), with the degree of infection correlating with depth. We then analyzed physical (light, temperature, salinity, mixed layer depth) and chemical (phosphate, nitrate and nitrite, ammonium, dissolved oxygen) aspects of this depth distribution to determine which parameters were the most robust predictors of the VMR–depth relationship. Light was the only significant ($P = 3.14 \times 10^{-4}$) and robust ($R^2 = 0.13$) predictor of VMR (Table 2; Fig. S8) across depth, whereas the other parameters were either not significant ($P > 0.05$) or only weakly (R^2 ranged from 0.04 to 0.06, often prone to the impact of outliers) related to VMR.

Discussion

Elucidating the cellular processes that fundamentally regulate EhV infection is essential for developing a mechanistic framework for interpreting and modeling algal host–virus interactions. Given their inability to replicate without a host, it follows that obtaining nucleotides, either through host genome recycling or *de novo* synthesis, represents the first and foremost challenge to viral production. As the primary mechanism for *de novo* nucleotide synthesis, an increased PPP activity during infection has been documented in a wide range of systems, including animals, plants, and cyanobacteria (Bissell *et al.*, 1973; Šindelář *et al.*, 1999; Lachaise *et al.*, 2001; Thompson *et al.*, 2011). Widespread enrichment of genes associated with the PPP has also been observed in marine metaviromes (Enav *et al.*, 2014).

Here, we show that EhV infection increases host PPP activity, consistent with increased PPP-associated gene expression (Rosenwasser *et al.*, 2014). We suggest this induced activity allows EhV to meet the requirement for genome replication that cannot be supported by host nucleotide recycling alone. With a genome size of *c.* 400 000 bp (Nissimov *et al.*, 2012) and burst sizes ranging from 500 to 1000 virions per host (this study; Castberg *et al.*, 2002), EhV201 would conservatively require 2×10^8 nucleotides for replication. Even if all 1.42×10^8 nucleotides of the *E. huxleyi* genome (Read *et al.*, 2013) were recycled, EhV would

still require an additional 6×10^7 nucleotides to achieve a mature burst size. This disparity becomes even more pronounced when the discrepancy between the guanine–cytosine content of *E. huxleyi* (66%) and EhV (40%) is taken into account. Although the plastid genome could also provide a source of recycled nucleotides, our observations of high PsbD expression (a gene encoded by the plastid genome) in infected cultures argues against plastid genome recycling.

The importance of *de novo* nucleotide synthesis is further supported by reduced RuBisCO protein levels and maintenance of electron transport rates and PSII activity. By diverting photosynthetic energy toward the PPP, viruses may enhance nucleotide synthesis while preserving energy that would otherwise be spent fixing unnecessary carbon. While functionally equivalent to similar observations in cyanophage (Lindell *et al.*, 2004; Thompson *et al.*, 2011), the mechanism by which EhV maintains host photosynthesis while decreasing RuBisCO is unclear.

Light-dependent adsorption and entry of EhV to host cells is conceptually similar to cyanophage (Cséke & Farkas, 1979; Kao *et al.*, 2005; Jia *et al.*, 2010), and we hypothesize this dependence is related to the role lipid rafts play in facilitating EhV entry (Rose *et al.*, 2014). Lipid rafts, membrane microdomains that sense extracellular stimuli and activate various signaling cascades through protein–protein interactions, have been implicated as entry sites of pathogens and viruses in other systems (Neilan *et al.*, 1999; Chazal & Gerlier, 2003; Hajishengallis & Lambris, 2011). Proteomic analysis of purified lipid rafts from infected *E. huxleyi* cells suggests EhVs utilize a similar entry mechanism (Rose *et al.*, 2014). Intriguingly, *E. huxleyi* lipids rafts were also found enriched in light-harvesting and Chl*a*/*b* binding proteins (Rose *et al.*, 2014). Although a role for lipid rafts in light capture is unknown, we posit that light regulates lipid raft production and thereby functionally limits entry of EhV during periods of darkness.

Viral replication and production were also impacted by light, with fewer viruses produced when infected cultures were maintained in the dark. As obligate photoautotrophs, prolonged

darkness represents a significant physiological stress, and the lack of viral production may simply be due to host senescence. However, if cell mortality was significant, we would expect a dramatic decrease in host abundance. Rather, we observed no net change in cell abundance, suggesting either equal growth and mortality or that cells were neither dividing nor dying. By contrast, when host cultures were maintained under continuous light, viral production was enhanced, further supporting the hypothesis that light is required for maximum viral production. In addition, elevated basal PPP activity in continuous light cultures compared with LD cultures suggests increased EhV production is supported by the availability of additional nucleotides through enhanced *de novo* synthesis.

Despite evidence that algal viruses have the potential to be a primary control on natural communities (Bratbak *et al.*, 1993; Schroeder *et al.*, 2003; Vardi *et al.*, 2012; Laber *et al.*, 2018; Sheyn *et al.*, 2018), their impacts are not quantitatively assessed in ecosystem models resolving coupled interactions between phytoplankton, grazers, and bacteria. This is in part due to the lack of empirical data on key parameters, such as encounter and adsorption with hosts (ϕ), replication rates (e.g. μ_v, μ'_v) and host lysis (δ) (Record *et al.*, 2016). Our empirically based mathematical model of EhV production hypothesizes that viral production is influenced by the rate of nucleotide recycling and *de novo* synthesis. In the dark, when host metabolism is suppressed, viral production is diminished due to a combination of rapid nucleotide recycling and diminished *de novo* synthesis. When hosts grow rapidly at intermediate irradiance, reduced host nucleotide recycling can support enhanced viral production because host integrity and growth are preserved, leading to a larger pool of available host nucleotides for viral genome replication. At high light, viral production is diminished due to a combination of rapid nucleotide recycling and diminished rates of *de novo* synthesis. Together, these insights form a base with which to explore ecosystem effects of host–virus metabolism in contrasting aquatic light environments.

Our laboratory-based data suggest EhV adsorption, and subsequent conversion and/or synthesis of nucleotides, is enhanced in the light and that maximum viral replication occurred at mid-range irradiance levels. At high light, viral production may be inhibited by high reactive oxygen species production (Sheyn *et al.*, 2016), whereas at low light there may simply not be enough *de novo* nucleotide synthesis to support high viral production. Alternatively, the shorter latent period (i.e. the time until host lysis) at the higher irradiance levels ($> 500\ \mu mol\ m^{-2}\ s^{-1}$) may itself represent an advantageous strategy whereby the virus induces host lysis to ensure virion release. This has been observed in bacteriophage, whereby the optimal lysis time is dependent on host abundance and physiology (Wang, 2006). We also cannot rule out a direct effect of light on the viruses. Although ultraviolet radiation is the major cause of viral decay in the ocean (Suttle & Chen, 1992; Noble & Fuhrman, 1997), photosynthetically active radiation has also been documented to facilitate decay (Traving *et al.*, 2014; Wei *et al.*, 2018). Exploring the effect of photosynthetically active radiation on viral abundance, infectivity, and adsorption needs

to be further investigated to better understand the mechanism by which light impacts the latent period and viral production. Regardless, our data suggest virus activity in the upper ocean may be vertically structured by light. Within stations, the highest intracellular EhV abundance measured in natural populations occurred at depths corresponding to *c.* 1–10% of the surface irradiance I_0, near the base of the euphotic zone, with lower abundances above and below this level. This was not due to the number of available hosts, given that VMR is normalized to host abundance; and importantly, these data are consistent with our laboratory findings that EhV replication is maximal between irradiances of 150 and 300 $\mu mol\ m^{-2}\ s^{-1}$, levels that would correspond to *c.* 7–15% surface I_0 on a sunny day (*c.* 2000 $\mu mol\ m^{-2}\ s^{-1}$). When the entire dataset is pooled (97 discrete samples across 2000 nautical miles) and tested against a variety of environmental parameters, light was the only one found to have a significant relationship with VMR, with increasing light leading to lower VMR. The somewhat low, but significant, R^2 value (0.13) may be partially attributed to sampled populations being at different stages of infection (Laber *et al.*, 2018), but nonetheless suggests a relationship between light and infection. Although we lose the resolution to disentangle the relationship seen at individual stations when we pool all of the samples, taken together with our laboratory data, these findings demonstrate that light can serve as a driving mechanism by which EhV infection can be vertically structured in natural populations.

Our laboratory-, field-, and modeling-based work form a mechanistic and empirical foundation on which to constrain key parameters regulating algal host–virus interactions. Our finding that light regulates critical aspects of EhV replication and production opens the door for mechanistic models of host–virus impacts on ecosystem function across a gradient of light environments. This, in turn, provides a novel and rigorous means to disentangle competing controls on phytoplankton populations, and the impact of viral infection on carbon cycling and nutrient dynamics.

Author contributions

KT and KDB conceived the study. KT designed the experiments. KT, LH, CM and JRL performed the experiments, DT and MJF performed the modeling. MJLC contributed the

quantitative PCR data from the North Atlantic field samples, FN performed the flow cytometry, BK analyzed the field data and contributed statistical analysis. KT, DT and KDB wrote the paper with contributions from BK, MJLC and MJF.

ORCID

Kay D. Bidle (iD) http://orcid.org/0000-0003-4170-412X
Marco J. L. Coolen (iD) http://orcid.org/0000-0002-0417-920X
David Talmy (iD) http://orcid.org/0000-0002-7335-2088

References

Agustí S, Satta MP, Mura MP, Benavent E. 1998. Dissolved esterase activity as a trace of phytoplankton lysis: evidence of high phytoplankton lysis rates in the northwestern Mediterranean. *Limnology and Oceanography* 43: 1836–1849.

Bidle KD, Haramaty L, Barcelos e Ramos J, Falkowski P. 2007. Viral activation and recruitment of metacaspases in the unicellular coccolithophore, *Emiliania huxleyi. Proceedings of the National Academy of Sciences, USA* 104: 6049–6054.

Bidle KD, Vardi A. 2011. A chemical arms race at sea mediates algal host–virus interactions. *Current Opinion in Microbiology* 14: 449–457.

Bissell MJ, White RC, Hatie C, Bassham JA. 1973. Dynamics of metabolism of normal and virus-transformed chick cells in culture. *Proceedings of the National Academy of Sciences, USA* 70: 2951–2955.

van Boekel WHM, Hansen FC, Riegman R, Bak RPM. 1992. Lysis-induced decline of a *Phaeocystis* spring bloom and coupling with the microbial foodweb. *Marine Ecology Progress Series* 81: 269–276.

Bratbak G, Egge JK, Heldal M. 1993. Viral mortality of the marine alga *Emiliania huxleyi* (Haptophyceae) and termination of algal blooms. *Marine Ecology Progress Series* 93: 39–48.

Brown CM, MacKinnon J, Cockshutt A, Villareal T, Campbell D. 2008. Flux capacities and acclimation costs in *Trichodesmium* from the Gulf of Mexico. *Marine Biology* 154: 413–422.

Brussaard CPD. 2004. Optimization of procedures for counting viruses by flow cytometry. *Applied and Environmental Microbiology* 70: 1506–1513.

Brussaard CPD, Riegman R, Noordeloos AAM, Cadée GC, Witte H, Kop AJ, Nieuwland G, Duyl FCv, Bak RPM. 1995. Effects of grazing, sedimentation and phytoplankton cell lysis on the structure of a coastal pelagic food web. *Marine Ecology Progress Series* 123: 259–271.

Castberg T, Thyrhaug R, Larsen A, Sandaa R-A, Heldal M, Van Etten JL, Bratbak G. 2002. Isolation and characterization of a virus that infects *Emiliania huxleyi* (Haptophyta). *Journal of Phycology* 38: 767–774.

Chazal N, Gerlier D. 2003. Virus entry, assembly, budding, and membrane rafts. *Microbiology and Molecular Biology Reviews* 67: 226–237.

Coolen MJL. 2011. 7000 years of *Emiliania huxleyi* viruses in the Black Sea. *Science* 333: 451–452.

Cséke CS, Farkas GL. 1979. Effect of light on the attachment of cyanophage AS-1 to *Anacystis nidulans. Journal of Bacteriology* 137: 667–669.

Enav H, Mandel-Gutfreund Y, Béjà O. 2014. Comparative metagenomic analyses reveal viral-induced shifts of host metabolism towards nucleotide biosynthesis. *Microbiome* 2: e9.

Evans C, Malin G, Mills GP, Wilson WH. 2006. Viral infection of *Emiliania huxleyi* (Prymnesiophyceae) leads to elevated production of reactive oxygen species. *Journal of Phycology* 42: 1040–1047.

Fuhrman JA. 1999. Marine viruses and their biogeochemical and ecological effects. *Nature* 399: 541–548.

Fulton JM, Fredricks HF, Bidle KD, Vardi A, Kendrick J, DiTullio GR, Mooy BASV. 2014. Novel molecular determinants of viral susceptibility and resistance in the lipidome of *Emiliania huxleyi. Environmental Microbiology* 16: 1137–1149.

Gelman A, Roberts GO, Gilks WR. 1996. Efficient metropolis jumping rules. In: Bernado JM, Berger JO, Dawid AP, Smith AFM, eds. *Bayesian statistics 5.* New York, NY, USA: Oxford University Press, 599–607.

Gilg IC, Archer SD, Floge SA, Fields DM, Vermont AI, Leavitt AH, Wilson WH, Martinez JM. 2016. Differential gene expression is tied to photochemical efficiency reduction in virally infected *Emiliania huxleyi. Marine Ecology Progress Series* 555: 13–27.

Gorbunov MY, Falkowski PG. 2005. Fluorescence induction and relaxation (FIRe) technique and instrumentation for monitoring photosynthetic processes and primary production in aquatic ecosystems. In: van der Est A, Bruce D, eds. *Photosynthesis: fundamental aspects to global perspectives.* Lawrence, KS, USA: Allen Press, 1029–1031.

Hajishengallis G, Lambris JD. 2011. Microbial manipulation of receptor crosstalk in innate immunity. *Nature Reviews Immunology* 11: 187–200.

Holligan PM, Fernandez E, Aiken J, Balch WM, Boyd P, Burkill PH, Finch M, Groom SB, Malin G, Muller K. 1993. A biogeochemical study of the coccolithophore, *Emiliana huxleyi*, in the North Atlantic. *Global Biogeochemical Cycles* 7: 879–900.

Hunter JE, Frada MJ, Fredricks HF, Vardi A, Van Mooy BAS. 2015. Targeted and untargeted lipidomics of *Emiliania huxleyi* viral infection and life cycle phases highlights molecular biomarkers of infection, susceptibility, and ploidy. *Frontiers in Marine Science* 2: https://doi.org/10.3389/fmars.2015.00081.

Jia Y, Shan J, Millard A, Clokie MRJ, Mann NH. 2010. Light-dependent adsorption of photosynthetic cyanophages to *Synechococcus* sp. WH7803. *FEMS Microbiology Letters* 310: 120–126.

Joassin P, Delille B, Soetaert K, Harlay J, Borges AV, Chou L, Riebesell U, Suykens K, Grégoire M. 2011. Carbon and nitrogen flows during a bloom of the coccolithophore *Emiliania huxleyi*: modeling a mesocosm experiment. *Journal of Marine Systems* 85: 71–85.

Kao CC, Green S, Stein B, Golden SS. 2005. Diel infection of a cyanobacterium by a contractile bacteriophage. *Applied and Environmental Microbiology* 71: 4276–4279.

Laber CP, Hunter JE, Carvalho F, Collins JR, Hunter EJ, Schieler BM, Boss E, More K, Frada M, Thamatrakoln K et al. 2018. Coccolithovirus facilitation of carbon export in the North Atlantic. *Nature Microbiology* 3: 537–547.

Lachaise F, Martin G, Drougard C, Perl A, Vuillaume M, Wegnez M, Sarasin A, Daya-Grosjean L. 2001. Relationship between posttranslational modification of transaldolase and catalase deficiency in UV-sensitive repair-deficient xeroderma pigmentosum fibroblasts and SV40-transformed human cells. *Free Radical Biology and Medicine* 30: 1365–1373.

Lehahn Y, Koren I, Schatz D, Frada M, Sheyn U, Boss E, Efrati S, Rudich Y, Trainic M, Sharoni S et al. 2014. Decoupling physical from biological processes to assess the impact of viruses on a mesoscale algal bloom. *Current Biology* 24: 2041–2046.

Lindell D, Sullivan MB, Johnson ZI, Tolonen AC, Rohwer F, Chisholm SW. 2004. Transfer of photosynthesis genes to and from *Prochlorococcus* viruses. *Proceedings of the National Academy of Sciences, USA* 101: 11013–11018.

Llewellyn CA, Evans C, Airs RL, Cook I, Bale N, Wilson WH. 2007. The response of carotenoids and chlorophylls during virus infection of *Emiliania huxleyi* (Prymnesiophyceae). *Journal of Experimental Marine Biology and Ecology* 344: 101–112.

Mackinder LCM, Worthy CA, Biggi G, Hall M, Ryan KP, Varsani A, Harper GM, Wilson WH, Brownlee C, Schroeder DC. 2009. A unicellular algal virus, *Emiliania huxleyi* virus 86, exploits an animal-like infection strategy. *Journal of General Virology* 90: 2306–2316.

Metropolis N, Rosenbluth AW, Rosenbluth MN, Teller AH, Teller E. 1953. Equation of state calculations by fast computing machines. *Journal of Chemical Physics* 21: 1087–1092.

Neilan JG, Borca MV, Lu Z, Kutish GF, Kleiboeker SB, Carrillo C, Zsak L, Rock DL. 1999. An African swine fever virus ORF with similarity to C-type lectins is non-essential for growth in swine macrophages *in vitro* and for virus virulence in domestic swine. *Journal of General Virology* 80: 2693–2697.

Nielsen MV. 1997. Growth, dark respiration and photosynthetic parameters of the coccolithophorid *Emiliania huxleyi* (Prymnesiophyceae) acclimated to different day length–irradiance combinations. *Journal of Phycology* 33: 818–822.

Nissimov JI, Worthy CA, Rooks P, Napier JA, Kimmance SA, Henn MR, Ogata H, Allen MJ. 2012. Draft genome sequence of four coccolithoviruses:

Emiliania huxleyi virus EhV-88, EhV-201, EhV-207, and EhV-208. *Journal of Virology* 86: 2896–2897.

Noble RT, Fuhrman JA. 1997. Virus decay and its causes in coastal waters. *Applied and Environmental Microbiology* 63: 77–83.

Read BA, Kegel J, Klute MJ, Kuo A, Lefebvre SC, Maumus F, Mayer C, Miller J, Monier A, Salamov A *et al.* 2013. Pan genome of the phytoplankton *Emiliania* underpins its global distribution. *Nature* 499: 209–213.

Record NR, Talmy D, Våge S. 2016. Quantifying tradeoffs for marine viruses. *Frontiers in Marine Science* 3: https://doi.org/10.3389/fmars.2016.00251.

Rose SL, Fulton JM, Brown CM, Natale F, Van Mooy BAS, Bidle KD. 2014. Isolation and characterization of lipid rafts in *Emiliania huxleyi*: a role for membrane microdomains in host–virus interactions. *Environmental Microbiology* 16: 1150–1166.

Rosenwasser S, Mausz MA, Schatz D, Sheyn U, Malitsky S, Aharoni A, Weinstock E, Tzfadia O, Ben-Dor S, Feldmesser E *et al.* 2014. Rewiring host lipid metabolism by large viruses determines the fate of *Emiliania huxleyi*, a bloom-forming alga in the ocean. *Plant Cell* 26: 2689–2707.

Schatz D, Shemi A, Rosenwasser S, Sabanay H, Wolf SG, Ben-Dor S, Vardi A. 2014. Hijacking of an autophagy-like process is critical for the life cycle of a DNA virus infecting oceanic algal blooms. *New Phytologist* 204: 854–863.

Schroeder DC, Oke J, Hall M, Malin G, Wilson WH. 2003. Virus succession observed during an *Emiliania huxleyi* bloom. *Applied and Environmental Microbiology* 69: 2484–2490.

Schroeder DC, Oke J, Malin G, Wilson WH. 2002. *Coccolithovirus* (*Phycodnaviridae*): characterisation of a new large dsDNA algal virus that infects *Emiliania huxleyi*. *Archives of Virology* 147: 1685–1698.

Sheyn U, Rosenwasser S, Ben-Dor S, Porat Z, Vardi A. 2016. Modulation of host ROS metabolism is essential for viral infection of a bloom-forming coccolithophore in the ocean. *ISME Journal* 10: 1742–1754.

Sheyn U, Rosenwasser S, Lehahn Y, Barak-Gavish N, Rotkopf R, Bidle KD, Koren I, Schatz D, Vardi A. 2018. Expression profiling of host and virus during a coccolithophore bloom provides insights into the role of viral infection in promoting carbon export. *ISME Journal* 12: 704–713.

Šindelář L, Šindelářová M, Burketová L. 1999. Changes in activity of glucose-6-phosphate and 6-phosphogluconate dehydrogenase isozymes upon potato virus Y infection in tobacco leaf tissues and protoplasts. *Plant Physiology and Biochemistry* 37: 195–201.

Suttle CA. 2007. Marine viruses: major players in the global ecosystem. *Nature Reviews: Microbiology* 5: 801–812.

Suttle CA, Chen F. 1992. Mechanisms and rates of decay of marine viruses in seawater. *Applied and Environmental Microbiology* 58: 3721–3729.

Thamatrakoln K, Bailleul B, Brown CM, Gorbunov MY, Kustka AB, Frada M, Joliot PA, Falkowski PG, Bidle KD. 2013. Death-specific protein in a marine diatom regulates photosynthetic responses to iron and light availability. *Proceedings of the National Academy of Sciences, USA* 110: 20123–20128.

Thompson LR, Zeng Q, Kelly L, Huang KH, Singer AU, Stubbe J, Chisholm SW. 2011. Phage auxiliary metabolic genes and the redirection of cyanobacterial host carbon metabolism. *Proceedings of the National Academy of Sciences, USA* 108: E757–E764.

Tian W-N, Pignatare JN, Stanton RC. 1994. Signal transduction proteins that associate with the platelet-derived growth factor (PDGF) receptor mediate the PDGF-induced release of glucose-6-phosphate dehydrogenase from permeabilized cells. *Journal of Biological Chemistry* 269: 14798–14805.

Townsend DW, Keller MD, Holligan PM, Ackelson SG, Balch WM. 1994. Blooms of the coccolithophore *Emiliania huxleyi* with respect to hydrography in the Gulf of Maine. *Continental Shelf Research* 14: 979–1000.

Traving SJ, Clokie MRJ, Middelboe M. 2014. Increased acidification has a profound effect on the interactions between the cyanobacterium *Synechococcus* sp. WH7803 and its viruses. *FEMS Microbiology Ecology* 87: 133–141.

Tyrell T, Merico A. 2004. *Emiliania huxleyi*: bloom observations and the conditions that induce them. In: Thierstein HR, Young JR, eds. *Coccolithophores: from molecular processes to global impact*. Berlin, Germany: Springer-Verlag, 75–97.

Valiela I. 1995. *Marine ecological processes*. New York, NY, USA: Springer-Verlag.

Vardi A, Haramaty L, Van Mooy BAS, Fredricks HF, Kimmance SA, Larsen A, Bidle KD. 2012. Host–virus dynamics and subcellular controls of cell fate in a natural coccolithophore population. *Proceedings of the National Academy of Sciences, USA* 109: 19327–19332.

Vardi A, Van Mooy BAS, Fredricks HF, Popendorf KJ, Ossolinski JE, Haramaty L, Bidle KD. 2009. Viral glycosphingolipids induce lytic infection and cell death in marine phytoplankton. *Science* 326: 861–865.

Wang I-N. 2006. Lysis timing and bacteriophage fitness. *Genetics* 172: 17–26.

Wei W, Zhang R, Peng L, Liang Y, Jiao N. 2018. Effects of temperature and photosynthetically active radiation on virioplankton decay in the western Pacific Ocean. *Scientific Reports* 8: 1525–1533.

Wikner J, Vallino JJ, Steward GF, Smith DC, Azam F. 1993. Nucleic acids from the host bacterium as a major source of nucleotides for three marine bacteriophages. *FEMS Microbiology Ecology* 12: 237–248.

Supporting Information

Additional Supporting Information may be found online in the Supporting Information section at the end of the article:

Fig. S1 Time course of host and viral abundance during a typical infection experiment.

Fig. S2 Additional host and EhV abundance data for dark and continuous light infection experiments.

Fig. S3 Additional EhV abundance and burst size data for infections at different irradiance levels.

Fig. S4 Fitted model simulations to adsorption experiments.

Fig. S5 Mathematical model capturing host–virus population dynamics in different light conditions.

Fig. S6 Sensitivity of key fitted parameters to the rate of virus adsorption (φ).

Fig. S7 Depth profile of *Emiliania huxleyi* and EhV abundance.

Fig. S8. Linear regression analysis of VMR and physical and chemical parameters measured across the North Atlantic.

Table S1 Model parameter definitions and units.

Please note: Wiley Blackwell are not responsible for the content or functionality of any Supporting Information supplied by the authors. Any queries (other than missing material) should be directed to the *New Phytologist* Central Office.